

Lyapunov-Based Dropout Deep Neural Network (Lb-DDNN) Controller

Saiedeh Akbari*, Emily J. Griffis*, Omkar Sudhir Patil*, Warren E. Dixon*

Abstract—Deep neural network (DNN)-based adaptive controllers can be used to compensate for unstructured uncertainties in nonlinear dynamic systems. However, DNNs are also very susceptible to overfitting and co-adaptation. Dropout regularization is an approach where nodes are randomly dropped during training to alleviate issues such as overfitting and co-adaptation. In this paper, a dropout DNN-based adaptive controller is developed. The developed dropout technique allows the deactivation of weights that are stochastically selected for each individual layer within the DNN. Simultaneously, a Lyapunov-based real-time weight adaptation law is introduced to update the weights of all layers of the DNN for online unsupervised learning. A non-smooth Lyapunov-based stability analysis is performed to ensure asymptotic convergence of the tracking error. Simulation results of the developed dropout DNN-based adaptive controller indicate a 38.32% improvement in the tracking error, a 53.67% improvement in the function approximation error, and 50.44% lower control effort when compared to a baseline adaptive DNN-based controller without dropout regularization.

Index Terms—Deep neural network, dropout, adaptive control, Lyapunov methods, nonlinear control systems.

I. INTRODUCTION

Empirical evidence indicates that deep neural networks (DNNs) can provide better function approximation than single layer neural networks [1]. Traditionally, DNN-based controllers are trained using offline training methods based on prior collected datasets. [2, Section 6.6]. Recent developments in [3]–[7] use Lyapunov-based methods to develop unsupervised online learning for all weights of a deep neural network (i.e., Lb-DNNs).

Unfortunately, both offline and Lb-DNNs can exhibit significantly degraded performance due to data overfitting. Another challenge that decreases generalization and performance of the trained DNN is co-adaptation, where multiple neurons, or even entire layers, become overly reliant on each other during the training process [8]. One effective approach to address these issues is through dropout regularization. Dropout was originally introduced by G. Hinton in [9] to prevent co-adaptation of feature detectors and improve the generalization performance of DNNs. Dropout regularization involves stochastically dropping out neurons during training, which helps prevent over-fitting,

enhances the overall function approximation performance, and efficiently allocates computational resources while updating the network’s weights [10], [11]. By setting the activation of certain individual weights to zero, dropout induces sparse representation in the network which reduces co-dependency in neurons. Moreover, dropouts can be viewed as training an ensemble of multiple DNNs with smaller width that are trained independently. Independence in the training has a regularizing effect and provides better generalization to new information. This intuitive reasoning is also applicable for using dropout in DNN-based adaptive control, since dropouts mitigate co-adaptation by reducing the number of weights influencing an adaptation law.

Although dropout regularization has been used for offline training of DNNs in results such as [12], [13], its application has been limited in real-time adaptive control settings. In [10], the dropout method is employed on a DNN to improve the training performance of inner layers in pseudo real-time, and through simulations, the study demonstrates the improved performance of a DNN-based adaptive controller with dropout. However, the pseudo real-time adaptation laws in [10] are not stability-driven but are rather based on a modular design where the stability analysis is primarily facilitated using robust control techniques.

This paper introduces a novel dropout technique aimed at enhancing the function approximation performance of a DNN-based adaptive controller that updates the weights of all layers of the DNN using the Lyapunov-based update law in [3] (i.e., a Lyapunov-based Dropout Deep Neural Network (Lb-DDNN)). The proposed technique involves the selective inactivation, or dropout, of weights associated with randomly selected neurons within each DNN layer. To incorporate dropout regularization, a new recursive DNN representation and stability-driven weight adaptation laws are constructed by considering the effect of randomization matrices on the closed-loop error system. Through a non-smooth Lyapunov-based stability analysis, the designed controller is guaranteed to stabilize the system in the sense that the tracking error asymptotically converges to zero. Simulation experiments are performed to compare the Lb-DDNN adaptive controller with the baseline adaptive DNN controller developed in [3]. The simulation results show a 35.56% improvement in the tracking error, a 49.94% improvement in the function approximation error, and 48.56% lower control effort in the proposed controller when compared to the baseline controller.

*Saiedeh Akbari, Emily J. Griffis, Omkar Sudhir Patil, and Warren E. Dixon are with the Department of Mechanical and Aerospace Engineering, University of Florida, Gainesville, FL, 32611-6250 USA. Email: {akbaris, emilygriffis00, patilomkarsudhir, wdixon}@ufl.edu.

This research is supported in part by AFRL grant FA8651-21-F-1027, AFRL grant FA8651-21-F-1025, AFOSR grant FA9550-19-1-0169, and Office of Naval Research grant N00014-21-1-2481. Any opinions, findings, and conclusions or recommendations expressed in this material are those of the author(s) and do not necessarily reflect the views of the sponsoring agencies.

II. PROBLEM FORMULATION

A. Notation

The space of essentially bounded Lebesgue measurable functions is denoted by \mathcal{L}_∞ . Given two functions $f : A \rightarrow B$ and $g : B \rightarrow C$, where A , B , and C are sets, the composition of f and g , denoted as $g \circ f$, is a new function $h : A \rightarrow C$ defined as $h \triangleq g \circ f = g(f(x))$, for all $x \in A$. Let $\mathbf{0}_{m \times n}$ denote a zero matrix with the dimension of $m \times n$. Let $I_{n \times n}$ denote an identity matrix with the dimension of n . For matrices $A \in \mathbb{R}^{m \times n}$ and $B \in \mathbb{R}^{p \times q}$, the Kronecker product is denoted as $A \otimes B$. Given a matrix $A \triangleq [a_{i,j}] \in \mathbb{R}^{n \times m}$, where $a_{i,j}$ denotes the element in the i^{th} row and j^{th} column of A , the vectorization operator is defined as $\text{vec}(A) \triangleq [a_{1,1}, \dots, a_{1,m}, \dots, a_{n,1}, \dots, a_{n,m}]^\top \in \mathbb{R}^{nm}$. From [14, Proposition 7.1.9] and given matrices $A \in \mathbb{R}^{p \times a}$, $B \in \mathbb{R}^{a \times r}$, and $C \in \mathbb{R}^{r \times s}$, the vectorization operator satisfies the property $\text{vec}(ABC) = (C^\top \otimes A) \text{vec}(B)$. Differentiating $\text{vec}(ABC)$ on both sides with respect to $\text{vec}(B)$ yields the property $\frac{\partial}{\partial \text{vec}(B)} \text{vec}(ABC) = C^\top \otimes A$. The right-to-left

matrix product operator is represented by $\overset{\wedge}{\prod}$, i.e., $\overset{\wedge}{\prod}_{p=1}^m A_p =$

$A_m \dots A_2 A_1$, and $\overset{\wedge}{\prod}_{p=a}^m A_p = 1$ if $a > m$. The Filippov set-valued map defined in [15, Equation 2b] is denoted by $\text{K}[\cdot]$. The notation $(\cdot)_{\text{a.a.t.}}$ denotes that the relation (\cdot) holds for almost all time (a.a.t.). Consider a Lebesgue measurable and locally essentially bounded function $h : \mathbb{R}^n \times \mathbb{R}_{\geq 0} \rightarrow \mathbb{R}^n$.

Then, the function $y : \mathcal{I} \rightarrow \mathbb{R}^n$ is called a Filippov solution of $\dot{y} = h(y, t)$ on the interval $\mathcal{I} \subseteq \mathbb{R}_{\geq 0}$ if y is absolutely continuous on \mathcal{I} and $\dot{y} \in \text{K}[h](y, t)$. Given some functions f and g , the notation $f(y) = \mathcal{O}^m(g(y))$ means that there exists some constants $M \in \mathbb{R}_{>0}$ and $y_0 \in \mathbb{R}$ such that $\|f(y)\| \leq M \|g(y)\|^m$ for all $y \geq y_0$. The operator $\text{proj}(\cdot)$ denotes the projection operator defined in [16, Appendix E, Eq. E.4].

B. Dynamic Model and Control Objective

Consider a control-affine nonlinear system modeled as

$$\dot{x}(t) = f(x(t)) + u(t), \quad (1)$$

where $t \in \mathbb{R}_{\geq 0}$, $x : \mathbb{R}_{\geq 0} \rightarrow \mathbb{R}^n$, $f : \mathbb{R}^n \rightarrow \mathbb{R}^n$, and $u : \mathbb{R}_{\geq 0} \rightarrow \mathbb{R}^n$ denote continuous time, the state, the unknown differentiable drift vector field, and the control input, respectively. The control objective is to design a controller $u(t)$ such that the state tracks the desired trajectory x_d . To achieve the control objective, an adaptive Lb-DNN architecture and a controller are designed to learn the unknown drift vector field and to achieve asymptotic convergence on the tracking error, respectively. To quantify the control objective, the tracking error $e : \mathbb{R}_{\geq 0} \rightarrow \mathbb{R}^n$, is defined as

$$e(t) \triangleq x(t) - x_d(t), \quad (2)$$

where $x_d : \mathbb{R}_{\geq 0} \rightarrow \mathbb{R}^n$ denotes a continuously differentiable desired trajectory.

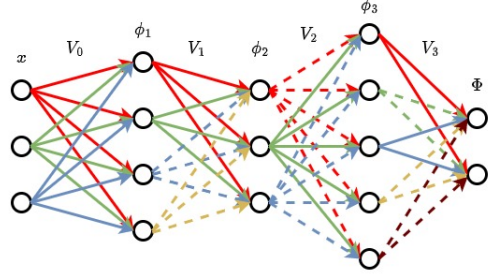


Figure 1. The structure of a DNN with three hidden layers, where the dashed and solid lines respectively represent the randomly dropped out and selected weights.

Assumption 1. The desired trajectory is designed such that for all $t \in \mathbb{R}_{\geq 0}$, $x_d(t) \in \Omega$, and $\dot{x}_d \in \mathcal{L}_\infty$, where $\Omega \subset \mathbb{R}^n$ is a known compact set. Hence, the desired trajectory can be bounded as $\|x_d\| \leq \bar{x}_d$, where $\bar{x}_d \in \mathbb{R}_{>0}$ is a known constant.

III. CONTROL DESIGN

A. Deep Neural Network Architecture

To estimate the unknown nonlinear drift vector field $f(x)$, a Lb-DNN architecture is developed using dropout. Dropout randomly omits neurons while training, which helps mitigate over-fitting and co-adaptation, thus improving the overall performance and function approximation capabilities of the DNN [10], [11]. Leveraging the Lyapunov stability-driven weight adaptation laws developed in [3], the dropout DNN is designed such that randomization matrices are used to incorporate dropout techniques into the online, stability-driven weight adaptation. Through the randomization matrices, weights associated with a batch of randomly selected neurons are inactivated, i.e., dropped out, to reduce the interdependency and excessive reliance on specific weights and neurons.

As shown in Figure 1, let the dropout DNN architecture, $\Phi : \mathbb{R}^n \times \{0, 1\}^{\sum_{m=0}^k L_m \times \sum_{m=0}^k L_m} \times \mathbb{R}^{\sum_{j=0}^k L_j L_{j+1}} \rightarrow \mathbb{R}^{L_{k+1}}$, be defined as

$$\Phi(x, R_i, \theta) = (R_{i,k} V_k)^\top \phi_k \circ \dots \circ (R_{i,1} V_1)^\top \phi_1 \circ (R_{i,0} V_0)^\top x, \quad (3)$$

where $k \in \mathbb{Z}_{>0}$ denotes the number of the layers in $\Phi(x, R_i, \theta)$, and $\phi_j : \mathbb{R}^{L_j} \rightarrow \mathbb{R}^{L_j}$ denotes the vector of smooth activation functions in the j^{th} layer, for all $j \in \{1, \dots, k\}$.¹ For $j \in \{0, \dots, k\}$, $V_j \in \mathbb{R}^{L_j \times L_{j+1}}$ and $L_j \in \mathbb{Z}_{>0}$ represent the weight matrix and the number of nodes in the j^{th} layer of Φ , respectively. For notation simplicity, the weights can be represented in a vector $\theta \in \mathbb{R}^{\sum_{j=0}^k L_j L_{j+1}}$ as $\theta \triangleq [\text{vec}(V_0)^\top, \text{vec}(V_1)^\top, \dots, \text{vec}(V_k)^\top]^\top$.

Let $R_i \in \{0, 1\}^{\sum_{m=0}^k L_m \times \sum_{m=0}^k L_m}$ denote the i^{th} instance of the randomization matrix, for all $i \in \mathcal{I} \triangleq \{1, \dots, J\}$, where \mathcal{I} denotes the set of all possible switching instances.

After every user-selected constant time period of $\delta t \in \mathbb{R}_{>0}$ seconds, the randomization matrix R_i switches to R_{i+1} , where

¹Although ϕ_j is defined as a smooth function, the subsequent analysis allows the inclusion of non-smooth activation functions by using the switched systems analysis in [3].

R_{i+1} is randomly selected from all possible permutations of randomization matrices. Each permutation is defined as

$$R_i \triangleq \begin{bmatrix} R_{i,0} & \mathbf{0}_{L_0 \times L_1} & \cdots & \mathbf{0}_{L_0 \times L_k} \\ \mathbf{0}_{L_1 \times L_0} & R_{i,1} & \cdots & \mathbf{0}_{L_1 \times L_k} \\ \vdots & \vdots & \ddots & \vdots \\ \mathbf{0}_{L_k \times L_0} & \mathbf{0}_{L_k \times L_1} & \cdots & R_{i,k} \end{bmatrix}, \quad \forall i \in \mathcal{I}.$$

For $i \in \{1, \dots, J\}$ and $j \in \{1, \dots, k\}$, $R_{i,j} \in \{0, 1\}^{L_j \times L_j}$ is designed to be a diagonal matrix, and the matrix $R_{i,0}$ is an identity matrix. The number of ones on the diagonal of each $R_{i,j}$ is equal to a user-selected constant number n_j , and the placement of non-zero elements on the diagonal of the matrix $R_{i,j}$ randomly changes after every δt seconds.² To illustrate the design of the randomization matrix $R_{i,j}$ and the effect of dropout on the DNN architecture, the following example is provided.

Example 1. Consider $R_{i,2} \in \{0, 1\}^{3 \times 3}$, $V_2 \in \mathbb{R}^{3 \times 2}$, and let $n_2 = 1$. Therefore, every δt seconds, $n_2 = 1$ of the elements on the diagonal of $R_{i,2}$ are randomly set to 1 and the others are zeroed. The considered permutations of $R_{i,2}$ for $i \in \{1, 2, 3\}$ are

$$R_{1,2} = \begin{bmatrix} 1 & 0 & 0 \\ 0 & 0 & 0 \\ 0 & 0 & 0 \end{bmatrix}, R_{2,2} = \begin{bmatrix} 0 & 0 & 0 \\ 0 & 1 & 0 \\ 0 & 0 & 0 \end{bmatrix}, R_{3,2} = \begin{bmatrix} 0 & 0 & 0 \\ 0 & 0 & 0 \\ 0 & 0 & 1 \end{bmatrix}.$$

Let $v_{p \times q} \in \mathbb{R}$ denote to each individual weight of the weight matrix V_2 , for rows $p \in \{1, 2, 3\}$ and columns $q \in \{1, 2\}$. For $p \in \{1, 2, 3\}$, let $\phi_{2,p} : \mathbb{R}^{L_2} \rightarrow \mathbb{R}^{L_2}$ denote to the activation functions of the second layer such that the activation vector is $\phi_2 = [\phi_{2,1}, \phi_{2,2}, \phi_{2,3}]^\top$. Therefore, in the presence and absence of dropout matrix $(R_{3,2}V_2)^\top \phi_2$ and $V_2^\top \phi_2$ are respectively obtained as

$$\begin{aligned} (R_{3,2}V_2)^\top \phi_2 &= \begin{bmatrix} v_{1,1} & v_{1,2} \\ v_{2,1} & v_{2,2} \\ v_{3,1} & v_{3,2} \end{bmatrix}^\top \begin{bmatrix} 0 & 0 & 0 \\ 0 & 0 & 0 \\ 0 & 0 & 1 \end{bmatrix}^\top \begin{bmatrix} \phi_{2,1} \\ \phi_{2,2} \\ \phi_{2,3} \end{bmatrix} \\ &= \begin{bmatrix} v_{3,1}\phi_{2,3} \\ v_{3,2}\phi_{2,3} \end{bmatrix}. \end{aligned} \quad (4)$$

$$\begin{aligned} V_2^\top \phi_2 &= \begin{bmatrix} v_{1,1} & v_{1,2} \\ v_{2,1} & v_{2,2} \\ v_{3,1} & v_{3,2} \end{bmatrix}^\top \begin{bmatrix} \phi_{2,1} \\ \phi_{2,2} \\ \phi_{2,3} \end{bmatrix} \\ &= \begin{bmatrix} v_{1,1}\phi_{2,1} + v_{2,1}\phi_{2,2} + v_{3,1}\phi_{2,3} \\ v_{1,2}\phi_{2,1} + v_{2,2}\phi_{2,2} + v_{3,2}\phi_{2,3} \end{bmatrix}. \end{aligned} \quad (5)$$

Comparing (4) and (5) suggests how the dropout method deactivates the activation functions associated with the zeros on the diagonal of the randomization matrix. Since the dropout matrix is randomly generated, a new batch of weights are selected every δt seconds.

The universal function approximation property states that the function space of (3) is dense in $\mathcal{C}(\mathcal{X})$, where $\mathcal{C}(\mathcal{X})$ denotes the space of continuous functions over the compact set $\mathcal{X} \subseteq \mathbb{R}^n$, where $x \in \mathcal{X}$ [17, Theorem 1.1]. Therefore, for all $j \in \{0, \dots, k\}$, there exists a corresponding vector of ideal weights $\theta^* \in \mathbb{R}^{\sum_{j=0}^k L_j L_{j+1}}$ such that $\sup_{x_d \in \Omega} \|f(x) - \Phi(x, R_i, \theta^*)\| \leq \bar{\varepsilon}$. Thus, the drift vector field can be modeled as

$$f(x) = \Phi(x, R_i, \theta^*) + \varepsilon(x), \quad (6)$$

²Once the system reaches the steady state, the randomization can be stopped in the sense that R_i is replaced with identity matrices. This can be considered as the final permutation of R_i for all $i \in \mathcal{I}$.

where $\varepsilon : \mathbb{R}^n \rightarrow \mathbb{R}^n$ denotes an unknown function reconstruction error that can be bounded as $\sup \|\varepsilon(x)\| \leq \bar{\varepsilon}$.

Assumption 2. The vector of ideal weights can be bounded by a known constant $\bar{\theta} \in \mathbb{R}_{>0}$ as $\|\theta^*\| \leq \bar{\theta}$, [18, Assumption 1].

B. Adaptation Law

To fulfill the tracking objective, the DNN model in (6) is used to estimate the unknown drift dynamics in (1). Since the ideal weights of the modeled DNN are unknown, adaptive estimates of the weight matrices are developed to learn the unknown drift dynamics $f(x)$. Let $\hat{\theta} : \mathbb{R}_{\geq 0} \rightarrow \mathbb{R}^{\sum_{j=0}^k L_j L_{j+1}}$ be defined as $\hat{\theta}(t) \triangleq \left[\text{vec}(\widehat{V}_0)^\top, \text{vec}(\widehat{V}_1)^\top, \dots, \text{vec}(\widehat{V}_k)^\top \right]^\top$,

where $\widehat{V}_j : \mathbb{R}^{L_j \times L_{j+1}}$, for all $j \in \{0, \dots, k\}$, denote the weight estimates. The corresponding weight estimation error $\tilde{\theta} : \mathbb{R}_{\geq 0} \rightarrow \mathbb{R}^{\sum_{j=0}^k L_j L_{j+1}}$ is defined as $\tilde{\theta}(t) \triangleq \theta^* - \hat{\theta}(t)$. Using the weight estimates $\hat{\theta}$, the adaptive estimate of $f(x)$ can be represented as $\Phi(x, R_i, \hat{\theta}) \triangleq (R_{i,k}\widehat{V}_k)^\top \phi_k \circ \dots \circ (R_{i,1}\widehat{V}_1)^\top \phi_1 \circ (R_{i,0}\widehat{V}_0)^\top x$. The estimated DNN architecture can be written in a recursive relation as

$$\widehat{\Phi}_j = \begin{cases} (R_{i,j}\widehat{V}_j)^\top \phi_j(\widehat{\Phi}_{j-1}), & j = \{1, \dots, k\}, \\ (R_{i,0}\widehat{V}_0)^\top x, & j = 0, \end{cases} \quad (7)$$

where $\widehat{\Phi}_j$ is the shorthand notation for $\widehat{\Phi}_j \triangleq \Phi_j(x, R_i, \hat{\theta})$, and $\widehat{\Phi} = \widehat{\Phi}_k$. Based on the subsequent stability analysis, the adaptation law for DNN weight estimates is designed as

$$\dot{\hat{\theta}} \triangleq \text{proj}(\Gamma_\theta \widehat{\Phi}'^\top e), \quad (8)$$

where $\Gamma_\theta \in \mathbb{R}^{\sum_{j=0}^k L_j L_{j+1} \times \sum_{j=0}^k L_j L_{j+1}}$ denotes a positive-definite adaptation gain matrix, and $\widehat{\Phi}'$ is a shorthand notation for the Jacobian $\widehat{\Phi}' \triangleq \frac{\partial \Phi(x, R_i, \hat{\theta})}{\partial \hat{\theta}}$. The Jacobian $\widehat{\Phi}'$ can be represented as $\widehat{\Phi}' \triangleq [\widehat{\Phi}'_0, \dots, \widehat{\Phi}'_k]$, where the shorthand notation $\widehat{\Phi}'_j$ is defined as $\widehat{\Phi}'_j \triangleq \frac{\partial \Phi_j(x, R_i, \hat{\theta})}{\partial \hat{\theta}}$, for all $j \in \{0, \dots, k\}$. The projection operator is incorporated in the update law to ensure

that $\hat{\theta}(t) \in \Lambda \triangleq \left\{ \theta \in \mathbb{R}^{\sum_{j=0}^k L_j L_{j+1}} : \|\theta\| \leq \bar{\theta} \right\}$, for all $t \geq 0$.

Since $\|\theta^*\| \leq \bar{\theta}$ and $\|\hat{\theta}\| \leq \bar{\theta}$, using the definition of $\tilde{\theta}$, it can be shown that $\|\tilde{\theta}\| \leq 2\bar{\theta}$. Using (7), the chain rule, and the properties of the vectorization operator, the Jacobians $\widehat{\Phi}'_0$ and $\widehat{\Phi}'_j$, for all $j = \{1, \dots, k\}$ and $i \in \mathcal{I}$, can respectively be calculated as

$$\begin{aligned} \widehat{\Phi}'_0 &\triangleq \left(\prod_{l=1}^k (R_{i,l}\widehat{V}_l)^\top \widehat{\phi}'_l \right) \left((x^\top R_{i,0}) \otimes I_{L_1} \right), \\ \widehat{\Phi}'_j &\triangleq \left(\prod_{l=j+1}^k (R_{i,l}\widehat{V}_l)^\top \widehat{\phi}'_l \right) \left((\widehat{\Phi}_j^\top R_{i,j}) \otimes I_{L_{j+1}} \right), \end{aligned} \quad (9)$$

where $\hat{\phi}_j$ and the Jacobian $\hat{\phi}'_j$ are the short-hand notations for $\hat{\phi}_j \triangleq \phi_j(\hat{\Phi}_{j-1})$ and $\hat{\phi}'_j \triangleq \phi'_j(\hat{\Phi}_{j-1}) = \frac{\partial \hat{\Phi}_j}{\partial \hat{\theta}}$, respectively.

Remark 1. The presence of matrix R_i for all $i \in \mathcal{I}$ in (9) mitigates co-adaptation by reducing the interdependency of weights in the adaptation law.

C. Closed-Loop Error System

The designed DNN estimate is used in the developed controller to approximate the unknown drift vector field in (1). By incorporating the developed adaptive DNN estimate, the controller in (10) is designed such that the state x tracks the desired trajectory x_d despite inactivation of weights associated with a randomly selected batch of neurons. Based on the subsequent stability analysis, the control input is designed as

$$u(t) \triangleq \dot{x}_d - \hat{\Phi} - k_e e - k_s \text{sgn}(e), \quad (10)$$

where $k_e, k_s \in \mathbb{R}_{>0}$ are constant control gains. Taking the time-derivative of (2) and substituting (1), (6), and the designed controller in (10) and canceling cross-terms yields the closed-loop error system as

$$\dot{e}(t) = \Phi(x, R_i, \theta^*) - \hat{\Phi} + \varepsilon(x) - k_s \text{sgn}(e) - k_e e. \quad (11)$$

To address the technical challenges in deriving adaptation the DNN weights, many results use Taylor series approximation based techniques [3], [5], [7], [18, Eq. 22]. Applying a first-order Taylor series approximation-based error model on $\Phi(x, R_i, \theta^*) - \hat{\Phi}$ yields

$$\Phi(x, R_i, \theta^*) - \hat{\Phi} = \hat{\Phi}'\tilde{\theta} + \mathcal{O}^2(\|\tilde{\theta}\|), \quad (12)$$

where $\mathcal{O}(\|\tilde{\theta}\|)$ denotes the higher-order terms that can be bounded as $\|\mathcal{O}^2(\|\tilde{\theta}\|)\| \leq \Delta$, where $\Delta \in \mathbb{R}_{>0}$ denotes a known constant [5, Eq. 18]. Substituting (12) into (11) yields

$$\dot{e} = \hat{\Phi}'\tilde{\theta} + \mathcal{O}^2(\|\tilde{\theta}\|) + \varepsilon(x) - k_s \text{sgn}(e) - k_e e. \quad (13)$$

To facilitate the subsequent stability analysis, let $z : \mathbb{R}_{\geq 0} \rightarrow \mathbb{R}^\psi$ denote the concatenated error system defined as

$$z(t) \triangleq \begin{bmatrix} e^\top(t), \tilde{\theta}^\top(t) \end{bmatrix}^\top, \quad (14)$$

where $\psi \triangleq n + \sum_{j=0}^k L_j L_{j+1}$. Additionally, let $\dot{z} = h(z, t)$, where $h : \mathbb{R}^\psi \times \mathbb{R}_{\geq 0} \rightarrow \mathbb{R}^\psi$ is as

$$h(z, t) \triangleq \begin{bmatrix} \hat{\Phi}'\tilde{\theta} + \mathcal{O}^2(\|\tilde{\theta}\|) \\ +\varepsilon(x) - k_s \text{sgn}(e) - k_e e \\ -\text{proj}(\Gamma_\theta \hat{\Phi}'^\top e) \end{bmatrix}. \quad (15)$$

IV. STABILITY ANALYSIS

Let $V_L : \mathbb{R}^\psi \rightarrow \mathbb{R}_{\geq 0}$ denote the Lyapunov function candidate defined as

$$V_L(z) \triangleq \frac{1}{2} e^\top e + \frac{1}{2} \tilde{\theta}^\top \Gamma_\theta^{-1} \tilde{\theta}. \quad (16)$$

Given the known constants $\underline{\alpha}, \bar{\alpha} \in \mathbb{R}_{>0}$, the Lyapunov function candidate satisfies the following inequality:

$$\underline{\alpha} \|z\|^2 \leq V_L(z) \leq \bar{\alpha} \|z\|^2. \quad (17)$$

Let the open and connected sets $\mathcal{B} \in \mathbb{R}^\psi$ and $\Upsilon \subseteq \mathcal{X}$ be defined as $\mathcal{B} \triangleq \left\{ \varsigma \in \mathbb{R}^\psi : \|\varsigma\| \leq \omega \sqrt{\underline{\alpha}/\bar{\alpha}} \right\}$ and $\Upsilon \triangleq \left\{ \varsigma \in \mathcal{X} : \|\varsigma\| < \bar{x}_d + \omega \right\}$. Theorem 1 uses the non-smooth analysis technique in [19] to establish the invariance properties of Fillipov solutions to \dot{z} and to guarantee asymptotic convergence of the tracking error, e .

Theorem 1. *The controller designed in (10) and the DNN update law developed in (8) guarantee asymptotic tracking error convergence for the dynamical system in (1) in the sense that $\lim_{t \rightarrow \infty} \|e(t)\| = 0$, given $\|z(t_0)\| \in \mathcal{B}$ and that the gain condition $k_s > \bar{\varepsilon} + \Delta$ is satisfied.*

Proof: Let ∂V_L denote the Clarke gradient of V_L defined in [20, p. 39]. Since the Lyapunov function candidate is continuously differentiable, $\partial V_L(z) = \{\nabla V_L(z)\}$, where ∇ denotes the standard gradient operator. From (15), it can be concluded that for all $i \in \mathcal{I}$, V_L satisfies the following differential equation

$$\begin{aligned} \dot{V}_L &\stackrel{\text{a.a.t.}}{\in} \bigcap_{\sigma \in \partial V_L(z)} \sigma^\top \mathbf{K}[h](z, t) \\ &= \nabla V_L^\top(z) \mathbf{K}[h](z, t) \\ &= e^\top \left(\hat{\Phi}'\tilde{\theta} + \mathcal{O}^2(\|\tilde{\theta}\|) + \varepsilon(x) - k_e e \right. \\ &\quad \left. - k_s \mathbf{K}[\text{sgn}(e)] \right) - \tilde{\theta}^\top \Gamma_\theta^{-1} \mathbf{K}[\text{proj}](\Gamma_\theta \hat{\Phi}'^\top e). \end{aligned} \quad (18)$$

Using [16, Lemma E.1.IV], the bounds on $\mathcal{O}^2(\|\tilde{\theta}\|)$ and $\varepsilon(x)$, the fact that $\mathbf{K}[\text{proj}](\cdot)$ is the set of convex combinations of $\text{proj}(\cdot)$ and (\cdot) , and therefore, $-\tilde{\theta}^\top \Gamma_\theta^{-1} \mathbf{K}[\text{proj}](\Gamma_\theta \hat{\Phi}'^\top e) \leq -\tilde{\theta}^\top \hat{\Phi}'^\top e$, and canceling cross terms, (18) can be upper-bounded as

$$\dot{V}_L \stackrel{\text{a.a.t.}}{\leq} -k_e \|e\|^2 - k_s \|e\| + \|e\|(\Delta + \bar{\varepsilon}), \quad \forall i \in \mathcal{I}.$$

Selecting the gain k_s according to the gain condition in Theorem 1 yields

$$\dot{V}_L \stackrel{\text{a.a.t.}}{\leq} -k_e \|e\|^2. \quad (19)$$

From the inequality obtained in (19), [19, Corollary 1] can be invoked to conclude that $z \in \mathcal{L}_\infty$ and $\lim_{t \rightarrow \infty} \|e(t)\| = 0$.

Due to the facts that $\hat{\Phi}$ is smooth for all $i \in \mathcal{I}$, $x \in \Omega$, and $\|\tilde{\theta}\| \leq \bar{\theta}$, $\hat{\Phi} \in \mathcal{L}_\infty$. Since $\dot{x}_d \in \mathcal{L}_\infty$, $e \in \mathcal{L}_\infty$, and $\hat{\Phi} \in \mathcal{L}_\infty$, $u \in \mathcal{L}_\infty$. To show that $x \in \mathcal{X}$, and therefore the universal function approximation property holds, let $\|z(t_0)\| \in \mathcal{B}$. Since $\|z(t_0)\| \leq \omega \sqrt{\underline{\alpha}/\bar{\alpha}}$, using (17), $\|e(t)\| \leq \omega$. Hence, using (2), $\|x\|$ can be bounded as $\|x\| \leq \bar{x}_d + \omega$. Therefore, if $z(t_0) \in \mathcal{B}$, then $x \in \Upsilon \subseteq \mathcal{X}$. ■

V. SIMULATION

To demonstrate the efficacy of the Lb-DDNN adaptive controller, simulations are performed on a three-dimensional nonlinear system, and f in (1) is modeled as

$$f = \begin{bmatrix} x_1 x_2^2 \tanh(x_2) + \sin(x_1)^2 \\ \cos(x_1 + x_2 + x_3)^3 - \exp(x_2)^2 + x_1 x_2 \\ x_3^2 \log(1 + \text{abs}(x_1 - x_2)) \end{bmatrix},$$

where $x \triangleq [x_1, x_2, x_3]^\top : \mathbb{R}_{\geq 0} \rightarrow \mathbb{R}^3$ denotes the system state. Three simulation experiments are performed for 10 sec with initial condition $x(0) = [5, 1, -5]^\top$. The desired trajectory is selected as $x_d(t) = [\sin(2t), -\cos(t), \sin(3t) + \cos(-2t)]^\top$. The DNN used in the simulations has $k = 7$ inner layers with $L = 10$ neurons in each hidden layer and contained hyperbolic tangent activation functions. The first set of simulations are performed to compare the baseline DNN-based adaptive controller in [3] and the Lb-DDNN adaptive controller in (8) and (10). The second set of simulations are performed to examine the effect of δt on the performance of the propose method. The third set of simulations are performed to compare the performance in the absence and presence of dropout deactivation after the transient period. In all simulations, the DNN weight estimates are initialized randomly from the normal distribution $\mathcal{N}(0, 10)$. The control gains in (10) are selected as $k_e = 10.5$ and $k_s = 1.5$. The learning gain for the baseline DNN is selected as $\Gamma_\theta = 100I_{670 \times 670}$. In the first two sets of simulations, the randomization is activated for the first 2 sec where the system is in the transient stage. After 2 sec, all the randomization matrices change to identity matrices. For the first 2 sec, the learning gain of the dropout DNN update law in (8) is selected as $\Gamma_\theta = 100I_{670 \times 670}$, and after 2 sec, the learning gain changes to $\Gamma_\theta = 40I_{670 \times 670}$. In the transient stage of the first and third set of simulations, the matrices R_i change to R_{i+1} every $\delta t = 0.1$ sec.

The performance results of the simulations are presented in Table I. As shown in the first subplot of Figure 2, the tracking error for the dropout DNN converges significantly faster than the baseline DNN. Specifically, the dropout DNN results in convergence to the final error after approximately 0.5 sec, roughly four times faster than that of the baseline controller. Despite the jump in the tracking error after the deactivation of the dropout of the DNN weights, the dropout DNN still yields the norm of the root mean square tracking error of 0.81, which shows a 38.32% improvement when compared to the baseline DNN adaptive controller. Moreover, the baseline DNN controller presents more oscillatory behavior within the transient period than the dropout DNN controller. The oscillatory behavior in the baseline DNN is due to interdependency of weights in the adaptation. However, as stated in Remark 1, the dropout DNN mitigates co-adaptation in the adaptation law, thus yielding less oscillatory behavior. As shown in the second subplot of Figure 2, the function approximation error for the dropout DNN controller rapidly converges after less than 0.2 sec but takes approximately 2 sec to converge with the baseline DNN controller. Although there is a jump in the function approximation error after the deactivation of the DNN, the dropout DNN controller demonstrated a 53.67% improvement in function approximation with the norm of the root mean square function approximation error of 19.44. Thus, the developed dropout adaptive DNN architecture resulted in better transient behavior and improved tracking and function approximation performance with a 50.44% lower control effort when compared to the baseline adaptive DNN controller developed in [3].

To examine the effect of selecting different δt , simulations

Table I
PERFORMANCE COMPARISON RESULTS

DNN Architecture	$\ e\ $	$\ f - \hat{\Phi}\ $	$\ u\ $
DNN	1.32	41.81	780.19
Dropout DNN	0.81	19.44	386.67
Dropout DNN, $\delta t = 0.2$ sec	0.88	23.87	461.83
Dropout DNN, $\delta t = 0.05$ sec	0.90	22.64	430.79
Dropout DNN, no dropout deactivation	0.78	20.40	399.93
Dropout DNN, dropout deactivation after 1 sec	0.86	20.00	387.32

are performed with $\delta t = 0.2$ sec and $\delta t = 0.05$ sec using the Lb-DDNN controller. As shown in Figure 3, reducing δt causes more spikes in the tracking and function approximation performances. Although the differences between the tracking and function approximation errors are not significant, reducing δt is found to cause more spikes in the plots, as shown in Figure 3.

The third set of simulations examine the performance of the developed dropout DNN controller under two cases; dropping out the neurons for the entire duration of the simulation, and deactivating dropout after 1 sec. As shown in Figure 4, for both cases, the difference between the tracking and function approximation performances are insignificant during the first second, as expected. Once the dropout is deactivated after 1 sec, there is an overshoot in both tracking and function approximation errors which does not occur when dropout is maintained throughout the simulation duration. However, not deactivating the dropout after the transient period leads to more spikes in both tracking and function approximation error in the steady state stage. Despite the increase in the tracking error, deactivation of the dropout in the steady state leads to lower control input and function approximation error as shown in Table I.

VI. CONCLUSION

A dropout DNN-based adaptive controller is developed for general continuous nonlinear systems. Leveraging the stability-derived DNN update law in [3] and inspired by the dropout technique, the developed dropout DNN controller improves function approximation performance and yields faster learning when compared to the DNN controllers without dropout. A Lyapunov-based stability analysis is performed to guarantee stability in the sense that the tracking error asymptotically converges to zero. Simulation results show 38.32% and 53.67% improvement in the tracking error and function approximation error, respectively, with a 50.44% reduced control effort when compared to the baseline adaptive DNN controller. Additional simulations showed the effect of dropout during both transient and steady state periods and how modifying dropout parameters, i.e., δt , can effect system performance. Using the established Lb-DDNN framework, future work can explore implementation questions related to the dropout regularization such as changes in δt , the number of neurons that are randomly selected, and dropout deactivation strategies.

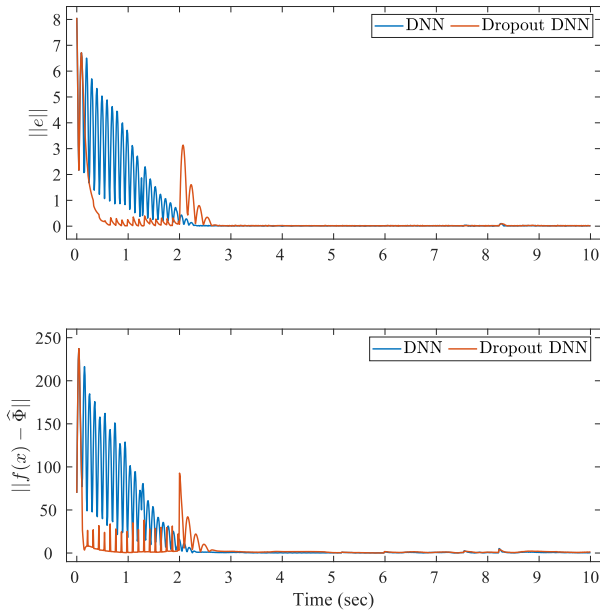


Figure 2. Performance of the tracking error (top) and function approximation error (bottom) over time comparing the Lb-DDNN controller and the adaptive DNN controller developed in [3].

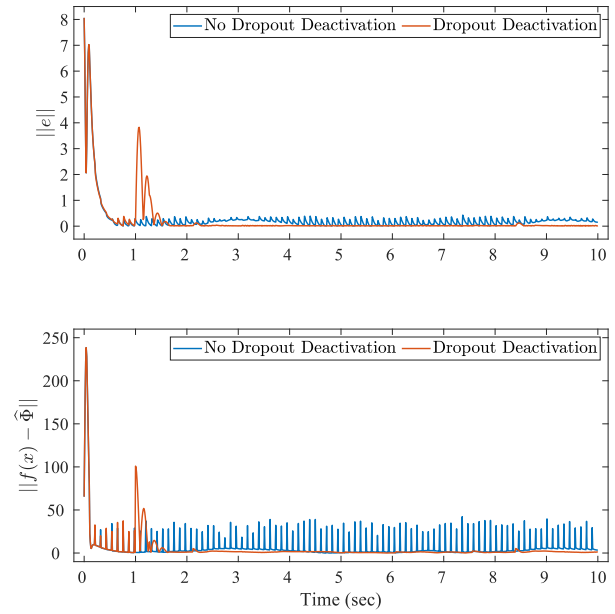


Figure 4. Performance of the tracking error (top) and function approximation error (bottom) over time in the presence and absence of dropout deactivation in the steady state (after 1 sec).

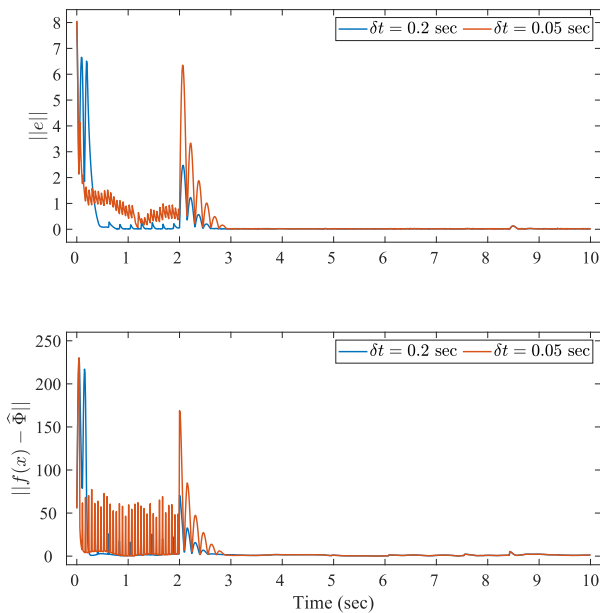


Figure 3. Performance of the tracking error (top) and function approximation error (bottom) over time for dropout DNN with two different δt values.

REFERENCES

- [1] S. Liang and R. Srikant, "Why deep neural networks for function approximation?," *arXiv preprint arXiv:1610.04161*, 2016.
- [2] S. L. Brunton and J. N. Kutz, *Data-driven science and engineering: Machine learning, dynamical systems, and control*. Cambridge University Press, 2019.
- [3] O. S. Patil, D. M. Le, E. Griffis, and W. E. Dixon, "Deep residual neural network (ResNet)-based adaptive control: A Lyapunov-based approach," in *Proc. IEEE Conf. Decis. Control*, 2022.
- [4] R. Sun, M. Greene, D. Le, Z. Bell, G. Chowdhary, and W. E. Dixon, "Lyapunov-based real-time and iterative adjustment of deep neural networks," *IEEE Control Syst. Lett.*, vol. 6, pp. 193–198, 2022.

- [5] O. Patil, D. Le, M. Greene, and W. E. Dixon, "Lyapunov-derived control and adaptive update laws for inner and outer layer weights of a deep neural network," *IEEE Control Syst. Lett.*, vol. 6, pp. 1855–1860, 2022.
- [6] G. Joshi and G. Chowdhary, "Deep model reference adaptive control," in *Proc. IEEE Conf. Decis. Control*, pp. 4601–4608, 2019.
- [7] E. Griffis, O. Patil, Z. Bell, and W. E. Dixon, "Lyapunov-based long short-term memory (Lb-LSTM) neural network-based control," *IEEE Control Syst. Lett.*, vol. 7, pp. 2976–2981, 2023.
- [8] C. A. Charu, *Neural networks and deep learning: a textbook*. Springer, 2018.
- [9] G. E. Hinton, N. Srivastava, A. Krizhevsky, I. Sutskever, and R. R. Salakhutdinov, "Improving neural networks by preventing co-adaptation of feature detectors," *arXiv preprint arXiv:1207.0580*, 2012.
- [10] D. Le, M. Greene, W. Makumi, and W. E. Dixon, "Real-time modular deep neural network-based adaptive control of nonlinear systems," *IEEE Control Syst. Lett.*, vol. 6, pp. 476–481, 2022.
- [11] N. Srivastava, G. Hinton, A. Krizhevsky, I. Sutskever, and R. Salakhutdinov, "Dropout: a simple way to prevent neural networks from overfitting," *J. Mach. Learn. Res.*, vol. 15, no. 1, pp. 1929–1958, 2014.
- [12] J. Ba and B. Frey, "Adaptive dropout for training deep neural networks," *Advances in neural inf. processing systems*, vol. 26, 2013.
- [13] G. E. Dahl, T. N. Sainath, and G. E. Hinton, "Improving deep neural networks for LVCSR using rectified linear units and dropout," in *Proc. IEEE Int. Conf. Acoust. Speech Signal Process.*, pp. 8609–8613, 2013.
- [14] D. S. Bernstein, *Matrix mathematics*. Princeton university press, 2009.
- [15] B. E. Paden and S. S. Sastry, "A calculus for computing Filippov's differential inclusion with application to the variable structure control of robot manipulators," *IEEE Trans. Circuits Syst.*, vol. 34, pp. 73–82, Jan. 1987.
- [16] M. Krstic, I. Kanellakopoulos, and P. V. Kokotovic, *Nonlinear and Adaptive Control Design*. New York: John Wiley & Sons, 1995.
- [17] P. Kidger and T. Lyons, "Universal approximation with deep narrow networks," in *Conf. Learn. Theory*, pp. 2306–2327, 2020.
- [18] F. L. Lewis, A. Yesildirek, and K. Liu, "Multilayer neural-net robot controller with guaranteed tracking performance," *IEEE Trans. on Neural Netw.*, vol. 7, no. 2, pp. 388–399, 1996.
- [19] N. Fischer, R. Kamalapurkar, and W. E. Dixon, "LaSalle-Yoshizawa corollaries for nonsmooth systems," *IEEE Trans. Autom. Control*, vol. 58, pp. 2333–2338, Sep. 2013.
- [20] F. H. Clarke, *Optimization and nonsmooth analysis*. SIAM, 1990.